Coupled simulations of turbulent flame and pyrolysis of combustible material

A. Snegirev*, E. Kokovina, A. Tsoy

Saint-Petersburg Polytechnic University, Polytechnicheskaya 29, Saint-Petersburg 195251 Russia

Abstract

Current practice of CFD fire modeling is still mainly based on uncoupled simulations of turbulent gaseous flame and gasification of combustible materials. Breaking the close feedback between both phenomena causes loss of the important information about real fire dynamics, impedes predicting material burning rates and flame spread over the fuel surface, ignores the critical conditions of ignition and extinction. The purpose of this work is to explore predictive potential of coupled simulations for ignition and burning of non-charring thermoplastic material (PMMA).

Using two recent versions of the FDS code (5.5 and 6.1) the following conclusions have been reached. Both models reveal good agreement between predicted times to ignition and published measurement data. Predicted dependence of steady burning rate on the external heat flux was found to be in qualitative agreement with the experimental data available, albeit important quantitative discrepancies have been identified. Two versions of the models also exhibited rather diverging results. Neither of the models used in this work replicated self-sustained burning of samples considered, except large sample burning simulated by FDS 5.5, for which predicted self-sustained burning rate was found to considerably exceed the experimental data available. Practical methodology of coupled simulations of self-sustained material burning has to be further elaborated to produce reliable predictions of burning rates.

1. Introduction

CFD fire modeling provides valuable information for quantitative risk assessment in fire safety. Comprehensive modeling is based on fundamental conservation laws and takes the properties of combustible materials into account.

Burning of solid combustibles in fires proceeds in close interaction of two very distinct phenomena: (i) thermal degradation of virgin material producing combustible volatiles and (ii) turbulent diffusion combustion of volatiles in oxidizing atmosphere. Two-way coupling of the above phenomena governs critical conditions of flame ignition and extinction, as well as the steady burning rate and the heat release rate.

Depending on consideration of this coupling, two different approaches are available.

1. In *uncoupled* simulations, combustible volatile production rate is preset using empirical data, which is equivalent to pre-assumed heat release rate per unit fuel surface area (HRRPUA). The solid phase model is therefore excluded, while the fire modeling is reduced to the gas phase modeling only.

2. In *coupled* simulations, both gas phase and solid phase models are jointly considered. Combustible volatiles are produced at a rate controlled by the net heat flux received by the fuel surface, heat transfer and pyrolysis reactions inside the fuel layer.

Coupling of two essentially different models for gas phase and solid material implies crucial importance of accurate prediction of the net heat flux received by the fuel. In self-sustained burning above fuel surface having dimensions of order of 0.2 – 1 m or larger, the net heat flux is mainly controlled by flame radiation. Accurate evaluation of the latter relies on quality of predicting flame shape, radiation emission, transfer and absorption. For smaller fuel sources, convective heat transfer dominates, and it raises requirements to spatial resolution of the boundary layer near the fuel surface.

To date, practical fire modeling is still mainly based on uncoupled simulations. Breaking the feedback between gas and solid phase phenomena causes loss of the important information about real fire dynamics [1]. Indeed, such an approach impedes predicting material burning rates and flame spread over the fuel surface, ignores the critical conditions of ignition and extinction. Rare existing examples of coupled simulations include numerical simulations of pre-ignition heating in cone calorimeter [2], piloted ignition of horizontal plate in the wind channel [3], flame spread over vertical [4] and horizontal [5] surfaces, burning of solid fuel in compartment [6], burning of wood cribs in [7]. In most of the abovementioned cases, simulation results did not demonstrate sufficient agreement with the measurement data. Advanced FireFOAM-based methodology of coupled simulations is currently developed in FM Global Research [8, 9].

The purpose of this work is to explore capability of two recent versions of FDS model (5.5 [10] and 6.1 [11]) in replicating ignition and burning of flammable solids using two-way coupling of turbulent combustion in gas flame and solid fuel pyrolysis.

2. Statement of the problem

We consider buoyant turbulent diffusion flame above the square horizontal surface of the combustible material. Fuel surface is heated by the external radiative heat flux. Fuel material undergoes thermal decomposition thereby producing combustible volatiles, which burn as they mix with the surrounding air.

Fuel layer thickness is set large enough to eliminate the heat transfer at the rear surface (thermally thick layer). Width of the fuel surface, D, varies from 0.1 to

* Corresponding author: a.snegirev@phmf.spbstu.ru

2 m. The fuel surface is placed in flash with the floor level being symmetrically located in the bottom surface of cubic computational domain. The bottom side of the computational domain is impermeable surface with constant temperature T_0 equal to that of surrounding air. All the side surfaces and the upper surface of the domain are open for the gas flow.

The simulations are presented for three scenarios.

1. Uncoupled simulations of the flame above the fuel surface with prescribed fuel supply rate. In these simulations, the effect of the fuel size, D, on fuel shape and structure, and on predicted radiative heat flux incident to the fuel surface is investigated.

2. Coupled simulations of material ignition and burning in test conditions of cone calorimeter. Times to ignition and steady burning rates are predicted for external heat fluxes in the range from 20 to 100 kW/m^2.

3. Coupled simulations of self-sustained burning with no external heat flux. The dependence of predicted burning rates on sample size is examined and compared to the experimental data.

3. Model description

3.1. Flame modelling

Two recent versions of the FDS model, 5.5 [10] and 6.1 [11], are applied and compared. In both cases, the Navier-Stokes equation system is solved in the low-Mach number limit. Poisson equation for modified pressure obtained by taking the divergence of the momentum equation is solved by a direct method using fast Fourier transforms. The large eddy simulation approach is used for the turbulence.

There are, however, important differences in discretization schemes used in solving transport equations and in subgrid turbulence models. In FDS 5.5, original procedure of scalar boundedness correction is applied, while in FDS 6.1 conventional TVD flux limiting procedure is used, with the Superbee limiter used by default. To model subgrid turbulence, the static Smagorinsky subgrid model, $\nu_{SGS} = (C_S\Delta)^2 S$, with C_S = 0.2 is used in FDS 5.5, and the variation of Deardorff's model, $\nu_{SGS} = C_V\Delta\sqrt{k_{SGS}}$, is applied (with the model constant of C_V = 0.1, and the subgrid kinetic energy, k_{SGS}, evaluated by averaging resolved velocity over adjacent cells).

For turbulent combustion modeling, the eddy dissipation concept is utilized in both models, and the single-step fast irreversible reaction is considered. Constant soot yield of 0.01 g soot per 1 g fuel is assumed. The rate of fuel consumption is set proportional to both the local limiting reactant concentration and the local rate of mixing. In FDS 5.5, the reaction time scale is inversely proportional to the resolved strain rate, $\tau_{mix} \sim 1/S$ (with the proportionality constant of 1.25, which is obtained from $\tau_{mix} = C\Delta^2/\mathscr{D}_{SGS}$, $\mathscr{D}_{SGS} = \nu_{SGS}/\mathrm{Sc}_T$, and $\nu_{SGS} = (C_S\Delta)^2 S$ with the default values C_S = 0.2 and Sc_T = 0.5). In FDS 6.1, the reaction time scale, is set minimum of diffusion, $\Delta^2/(\mathscr{D} + \mathscr{D}_{SGS})$, subgrid mixing, $\Delta/\sqrt{2k_{SGS}}$, and buoyancy, $\sqrt{2\Delta/g}$, time scales.

In both models, radiative transfer is simulated by solving the radiative transfer equation using the finite volume method with 104 discrete solid angles. Spectral properties of the gas-soot media are accounted for by the mean (gray) absorption coefficients, which are simulated by the RadCal procedure as a function of composition and temperature. In FDS 5.5, the emission term is evaluated as $\kappa I_b = \max\left(f_r \dot{q}'''/4\pi, \kappa\sigma T^4/\pi\right)$. In FDS 6.1, the relation $I_b = C\sigma T^4/\pi$ is used in all the grid cells, and the correction coefficient, C, is evaluated to ensure the ratio of the radiation emission in the flame to the chemical heat release to be equal to the pre-assumed radiative fraction, f_r (which is set to 0.35 in both models).

Thus, the major differences in the two models include those in treating convection terms in scalar transport equations, subgrid turbulence models, reaction time scales, and in evaluating radiation emission.

3.2. Fuel pyrolysis modeling

1D heat transfer equation,

$$c\rho\frac{\partial T}{\partial t} = \frac{\partial}{\partial x}\left(\lambda\frac{\partial T}{\partial x}\right) + \dot{q}_g''' + \dot{q}_r''' \,. \qquad (1)$$

is solved in the material layer in the direction normal to the exposed fuel surface. Boundary condition at the fuel surface takes into account conductive heat transfer to the material, absorbed radiation, reradiation, and the convective heat flux from the gas phase.

Transparency of the material for the radiative flux is accounted for. Radiative energy transfer and volumetric absorption is evaluated by the two-flux method. Contribution of radiation absorption in the material is represented by the radiation term $\dot{q}'''$ in Eq. (1).

Heat sink in endothermic thermal decomposition is represented in Eq. (1) by the gasification term,

$$\dot{q}_g''' = -\rho\Delta h_g \dot{r} \,, \qquad (2)$$

where ρ is the material density, Δh_g is the heat of gasification, and $\dot{r}$ is the pyrolysis reaction rate. The pyrolysis model assumes single-step first-order reaction,

$$\dot{r} = A(1-\alpha)\exp\left(-E_a/\mathscr{R}T\right), \qquad (3)$$

where $\alpha = (\rho_0 - \rho)/\rho_0$ is conversion.

In this work, we have only considered non-charring thermoplastic material, polymethyl methacrylate (PMMA). For this material, extensive experimental data is available on its pyrolysis, ignition and burning. Based on the literature data, thermal conductivity, density, and specific heat were taken, respectively, λ = 0.21 W/(m·K), ρ = 1190 kg/m^3, and c_P = 1.377 kJ/(kg·K). Fuel surface emissivity was set ε = 0.9.

Pyrolysis kinetic reaction rate, Eq. (3), was simulated with kinetic parameters A = 8.5·10^{12} s^{-1},

E_a = 188 kJ/mol [10]. Heat of gasification was set Δh_g = 870 kJ/g, unless specified otherwise.

3.3. Computational domain and mesh density

Cubic computational domain had the height equal to the doubled flame height evaluated from the Heskestad' relation, $L_f = 0.235\dot{Q}^{2/5} - 1.02D$ [12], where $\dot{Q}$ is the flame heat release rate (in kW). The heat release rate was obtained for the given sample size, D, and the HRRPUA value of 500 kW/m^2, typical for steady burning of large samples. As a result, for the sample sizes of 0.1, 0.5, 1.0 and 2.0 m the computational domain had the sizes of 0.7, 2.2, 3.6 and 5.8 m, respectively.

In all the cases, uniform Cartesian computational mesh was used having 80^3 = 512 000 grid cells. The ratio, D^*/Δ, where $D^* = \left(\dot{Q}/\left(\rho_{air,0} c_{P,air} T_0 \sqrt{g}\right)\right)^{2/5}$, varies from 13 to 18 for the sample sizes considered.

4. Simulation results

4.1. Prescribed fuel supply rate

In this scenario, the value of HRRPUA equal to 500 kW/m^2 is assumed. Instantaneous resolved iso-surfaces of 200 kW/m^3 and temperature distributions in the axial plane are illustrated in Fig. 1, where the simulation results are shown for both of the models used. Dashed straight lines show the flame height corresponding to the Heskestad' formula.

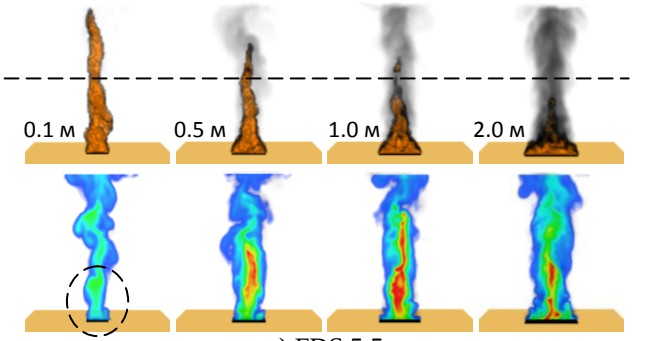

a) FDS 5.5

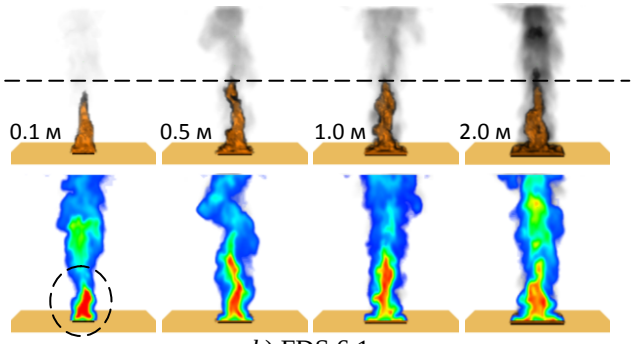

b) FDS 6.1

Fig. 1. Predicted instantaneous iso-surfaces of volumetric heat release rate 200 kW/m^3 and temperatures in the axial plane.

Opposite trends are observed for the flame height predictions by different models when the fuel sample size is reduced. Indeed, for the 0.1 m sample, FDS 5.5 predicts heavily elongated flame with overestimated flame height. Accordingly, predicted flame temperature *near the sample surface* (dashed circles) appears to be underestimated, compared to the prediction by FDS 6.1.

This is further illustrated by the predicted mean temperature distributions along the flame axis, which are compared in Fig. 2 with the measurements [13, 14]. It can be seen that the temperatures predicted by FDS 5.5 are well below the measured temperature range (corrected for thermocouple radiation), and the discrepancy increases for smaller sample sizes. In contrast, predictions by FDS 6.1 are in better agreement with the measurements.

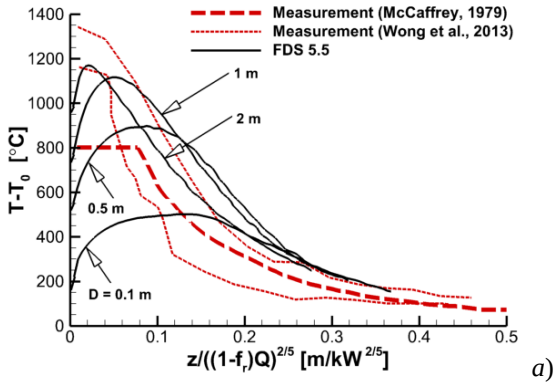

a)

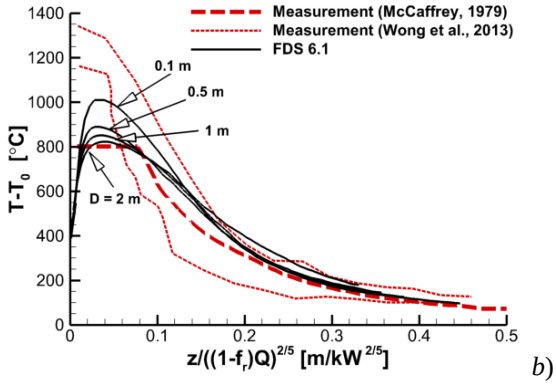

b)

Fig. 2. Mean axial temperature. Dashed lines – measurements [13, 14], solid lines – simulations. *a*) – FDS 5.5, *b*) – FDS 6.1.

Flame temperature distributions correlate with predicted heat fluxes received by the sample surface shown in Fig. 3.

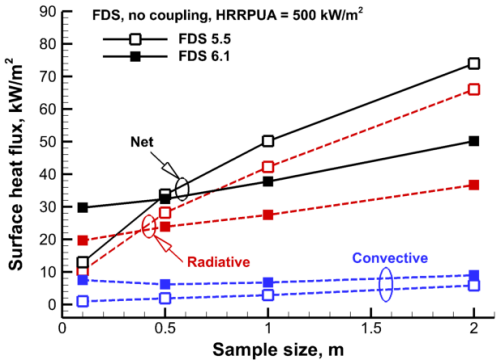

Fig. 3. Predicted heat fluxes at sample surface.

FDS 5.5 predicts strong dependence of the net heat flux on the sample size. Low flame temperatures near to the fuel surface for small samples result in underestimated heat flux incident to the surface. It can be seen in Fig. 3 that for small samples the net heat flux may not be sufficient to sustain the flame above the sample (in contrast with the experimental observations). In the opposite limit of large sample sizes, predicted net heat flux increases greatly, which could result in overestimated burning rates in coupled simulations.

FDS 6.1 predicts much weaker dependence of the net heat flux on the sample size, compared to FDS 5.5, mainly due to the radiative component also shown in Fig. 3.

4.2. Ignition and burning of the sample exposed to external heat flux

Cone calorimeter test conditions are considered, and flame simulations are undertaken jointly with the material pyrolysis. Sample surface (width is 0.1 m) is exposed to the spatially uniform heat flux, which is kept constant in time. A comparison of predicted and measured mass loss rates is shown in Fig. 4.

Simulation results include transient dependencies of the sample mass loss rate (Fig. 5, a) the surface temperature (Fig. 5, b), dependencies of time to ignition (Fig. 6, a), surface temperature at ignition (Fig. 6, b), and of steady mass loss rate (Fig. 7) on the external heat flux. All the above quantities are evaluated for the external heat fluxes from 20 to 100 kW/m^2, which is the range characteristic of real fires and fire tests in cone calorimeter.

4.2.1. Ignition

Predicted and measured dependencies of time to ignition and surface temperature at ignition on the external heat flux is shown in (Fig. 6). We assume that flaming ignition occurs as soon as the mass loss rate exceeds the value of 5 g/(m^2·s). It is worthy of note that predictions by FDS 5.5 and 6.1 are very close to each other. This is expected, since no flame exists prior to ignition, and the solid phase models are similar for both code versions. According to Fig. 6, *a*, surface temperature at ignition is practically constant. This observation justifies application of the thermal theory according to which flaming ignition occurs at time instant t_{ign} when the surface temperature approaches critical value, T_{ign}, being the material property. The thermal theory also assumes constancy of the net heat flux,

$$q''_{net} = \varepsilon q''_{ext} + q''_{conv} - q''_{rr}, \qquad (4)$$

received by the sample. In Eq. (4), q''_{ext} is the external heat flux, $q''_{rr} = \varepsilon\sigma T^4$ is the surface reradiation, q''_{conv} is the convective heat flux received by the sample. Setting $-\lambda\partial T/\partial x|_{surf}$ = q''_{net} = const, $\dot{q}'''_g$ = 0 and $\dot{q}'''_r$ = 0, the following expression for t_{ign} is obtained by solving Eq. (1) in thermally thick limit:

$$\frac{1}{\sqrt{t_{ign}}} = \sqrt{\frac{4}{\pi}\frac{1}{\lambda c\rho}}\frac{q''_{net}}{T_{ign}-T_0} = \frac{q''_{ext}-q''_{ext,cr}}{TRP} \qquad (5)$$

where

$$q''_{ext,cr} = \frac{1}{\varepsilon}\left(q''_{rr} - q''_{conv}\right) \approx \frac{1}{\varepsilon}q''_{rr} = \sigma T_{ign}^4 \qquad (6)$$

is the critical heat flux below which ignition does not occur at any duration of exposure, and

$$TRP = \frac{1}{\varepsilon}\sqrt{\frac{\pi}{4}\lambda c\rho}\left(T_{ign}-T_0\right) \qquad (7)$$

is the thermal response parameter [15].

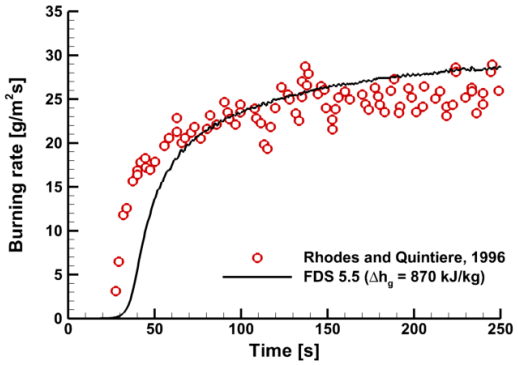

Fig. 4. Transient burning rate of 0.1x0.1 m PMMA plate exposed to 50 kW/m^2 heat flux.

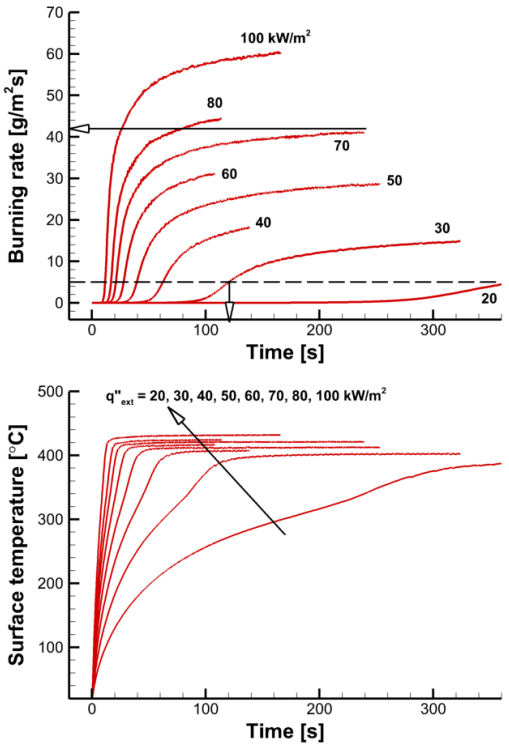

Fig. 5. Predicted transient dependencies of burning rate (*a*) and surface temperature (*b*) at different heat fluxes. FDS 5.5, 0.1x0.1 m PMMA plate. In top figure, vertical arrow shows ignition at critical mass loss rate of 5 g/(m^2·s), horizontal arrow shows steady burning rate.

The dependence of $t_{ign}^{-1/2}$ on q''_{ext}, calculated from Eq. (5), is shown by the dash-dot line in Fig. 7, *b*. Prediction by the thermal theory coincides with the FDS results at low external heat flux and increasingly overestimates the latter at higher heat fluxes. This is explained by the material transparency for the external heat flux, which is ignored by the thermal theory and taken into account by FDS. Similar result was obtained in [16].

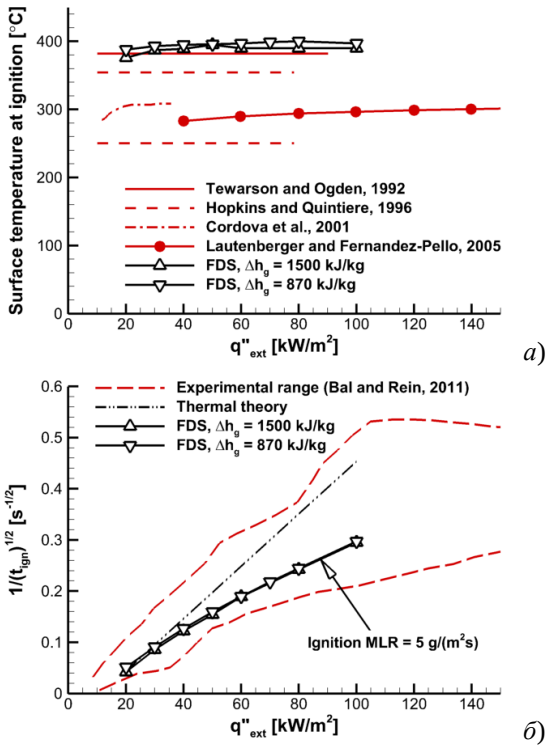

Fig. 6. Predicted and measured dependencies of surface temperature at ignition (*a*) and time to ignition (*b*) on external heat flux. Experimental data from [15, 16, 17, 18, 19].

Since the pyrolysis rate prior to ignition is low, both surface temperature and time to ignition are not sensitive to the heat of gasification. Surface temperatures at ignition (averaged over the considered range of external heat fluxes) is T_{ign} = 396°C for Δh_g = 870 kJ/kg and T_{ign} = 389 °C for Δh_g = 1500 kJ/kg. For the critical heat flux, Eq. (6), it results in $q''_{ext,cr} \approx \sigma T_{ign}^4 \approx 11.1$ kW/m^2, which is in agreement with the measurements [15].

Thus, material ignition by the external heat flux is predicted reasonably well. Recall, that in this scenario turbulent flame does not yet exist, having no thermal impact on fuel surface.

4.2.2. Steady burning

Steady burning rates of PMMA samples exposed to radiative heating in the cone calorimeter were measured in Refs [20–22]. In Fig. 7, these measurements are compared with the simulation results obtained in this work.

In addition to the flux components shown in Eq. (4) for pre-ignition heating, the net heat flux in steady burning also includes radiative heat flux from the flame, q''_{flame}:

$$q''_{net} = \varepsilon\left(q''_{ext} + q''_{flame}\right) + q''_{conv} - q''_{rr} \,. \qquad (8)$$

Using Eq. (8), the steady burning rate can be estimated from the heat balance at the fuel surface, $q''_{net} = \dot{m}''_{fuel}\Delta h_g$:

$$\dot{m}''_{fuel} = \frac{q''_{net}}{\Delta h_g} = \frac{\varepsilon}{\Delta h_g} q''_{ext} + \left(\varepsilon q''_{flame} + q''_{conv} - \varepsilon\sigma T^4\right). \qquad (9)$$

Although FDS predictions shown in Fig. 7 appear to be remarkably different for two models used, both dependencies exhibit the same slope, which is greater than that for the experimental trends. It might be an indication of underestimated heat of gasification which is indeed close to the lower bound of the literature data. Nevertheless, material property data set used in this work produced good agreement of steady burning rate predictions by FDS 5.5 with the measurements for heat fluxes around 50 kW/m^2. However, extrapolation of the dependence predicted by FDS 5.5 to q''_{ext} = 0 falls in the range of negative mass loss rates. It implies that FDS 5.5 (with the PMMA properties listed above) is unable to predict self-sustained burning of PMMA sample of 0.1 m. The latter is because of underestimated bracketed term in Eq. (9), and this is consistent with the underestimated flame temperature observed above in the simulations with prescribed burning rate.

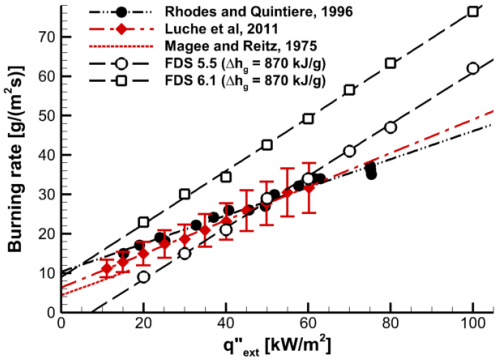

Fig. 7. Predicted and measured dependencies of burning rate on external heat flux. Experimental data from [20 - 22].

Alternatively, FDS 6.1 predicts positive values of the mass loss rate extrapolated to q''_{ext} = 0, being similar to those measured in the experiments. A possible reason of overestimated mass loss rates predicted by FDS 6.1 (Fig. 7) is the underestimated PMMA specific heat corresponding to the lower boundary of literature data.

4.2.3. Self-sustained burning

Ability of the model to predict self-sustained burning correctly has been assessed in this series of coupled simulations. Switching the external heat flux off makes the thermal feedback (between the heat release rate in turbulent flame and material gasification rate) to be the only driving force for burning.

In the simulations, samples were exposed to the external heat flux of 50 kW/m^2 until the steady burning

was established. The external heat flux was then switched off, and subsequent simulations were conducted until the steady regime (either extinction or steady self-sustained burning) was reached.

Simulation results have shown that neither of FDS models used in this work replicated self-sustained burning of samples considered, except large sample burning simulated by FDS 5.5. For large samples with D = 2 m, FDS 5.5 predicted steady burning rate of $\dot{m}''_{fuel}$ = 55 g/(m^2·s), which is approximately twice as higher as the experimental data [23].

The reason of such a remarkable disagreement with the experimental data on self-sustained burning of PMMA slabs is yet to be identified. The effect of near-wall grid resolution on the predicted heat fluxes incident to the sample surface, as well as performance of the pyrolysis model have to be examined.

5. Conclusions

Flaming ignition and burning of square PMMA samples has been investigated numerically using two versions of FDS models, both in uncoupled and coupled simulation scenarios. Samples with sizes ranging from 0.1 to 2 m have been examined either exposed to external heat flux (cone calorimeter conditions) or burning in self-sustained mode.

Improvements introduced in the most recent version of the FDS model have led to better agreement of predicted flame heights and of mean flame temperatures in the vicinity of fuel surface. Among the differences documented in [10] and [11], the most influential are those in treating convection terms in scalar transport equations, subgrid turbulence models, reaction time scales, and in evaluating radiation emission. The net heat flux received by the fuel surface from flame with prescribed fuel supply rate also appeared to be considerably different when it was predicted by FDS 5.5 and 6.1.

Good agreement has been obtained between predicted times to ignition and published measurement data. Simplified thermal theory has shown good performance for low external heat fluxes (below 30-40 kW/m^2) and produced greatly overestimated results (compared to FDS simulations) for higher heat fluxes. Such a discrepancy is attributed to the effect of material transparency for radiative heat flux.

Predicted dependence of steady burning rate on the external heat flux was found to be in qualitative agreement with the experimental data available, albeit important quantitative discrepancies have been identified. Two versions of the models also exhibited rather different results. Neither of the models used in this work replicated self-sustained burning of samples considered, except large sample burning simulated by FDS 5.5, for which predicted self-sustained burning rate was found to considerably exceed the experimental data available.

It can therefore be concluded that, despite of the powerful numerical tools developed to date and widely used in engineering practice, practical methodology of coupled simulations of self-sustained material burning is yet to be elaborated.

References

[1]. K. McGrattan, R. McDermott, J. Floyd, S. Hostikka, G. Forney, H. Baum. Int. J. Comp. Fluid Dynamics 26 (2012) 349-361.

[2]. T.-H. Tsai, M.-J. Li, I-Y. Shih, R. Jih, S.-C. Wong. Combust. Flame 124 (2001) 466-480.

[3]. S. Fereres, C. Lautenberger, A.C. Fernandez-Pello, D.L.Urban, G.A. Ruff. Combust. Flame 159 (2012) 3544-3553.

[4]. J.-W. Kwon. Evaluation of FDS V.4: Upward Flame Spread. MSc Thesis in Fire Protection Engineering, Worcester Polytechnic Institute, 2006. 118 P.

[5]. K.R. Prasad, R. Kramer, N. Marsh, M.R. Nyden. Numerical Simulation of Fire Spread on Polyurethane Foam Slabs // Fire and Materials 2009. 11th Int. Conference. Conference Papers. Proceedings. January 26-28, 2009, San Francisco, CA, Interscience Communications Ltd, London, England, 697-708 pp.

[6]. S. Yuan, J. Zhang. Fire Safety J. 44 (2009) 349-362.

[7]. C. Lautenberger. Gpyro3D: A Three Dimensional Generalized Pyrolysis Model. In: Fire Safety Science – Proc. of the 11th Int. Symp., IAFSS, 2014.

[8]. Y. Wang, K.V. Meredith, X. Zhou, P. Chatterjee, Y. Xin, M. Chaos, N. Ren, S.B. Dorofeev. Numerical Simulation of Sprinkler Suppression of Rack Storage Fires. In: Fire Safety Science – Proc. of the 11th Int. Symp., IAFSS, 2014.

[9]. M. Chaos, M.M. Khan, N. Krishnamoorthy, J.L. de Ris, S.B. Dorofeev. Proc. Combust. Inst. 33 (2011) 2599-2606.

[10]. R. McDermott, K. McGrattan, S. Hostikka, J. Floyd. Fire Dynamics Simulator (Version 5). Technical Reference Guide. Vol. 1-3. NIST Special Publication 1018-5, 2010.

[11]. K. McGrattan, S. Hostikka, R. McDermott, J. Floyd, C. Weinschenk, K. Overholt. Fire Dynamics Simulator Technical Reference Guide. FDS version 6.1. NIST Special Publication 1018, Sixth ed., 2014.

[12]. G. Heskestad. Fire Plumes, Flame Height, and Air Entrainment. SFPE Handbook of Fire Protection Engineering. 3rd ed. Quincy MA: NFPA, 2002. P. 2-1–2-17.

[13]. B.J. McCaffrey. Purely buoyant diffusion flames: some experimental results, NBSIR 79-1910, National Bureau of Standards, Washington D.C. 49 P.

[14]. W.C.-K. Wong, N.A. Dembsey, J. Alston, C. Lautenberger. J. Fire Prot. Engng. 23 (2013) 85-134.

[15]. A. Tewarson. Flammability. In: Physical Properties of Polymers Handbook. 2nd Edition, Ed. by J.E. Mark, Springer, 2007, pp. 889-925.

[16]. N. Bal, G. Rein. Combust. Flame 158 (2011) 1109-1116.

[17]. D. Hopkins Jr, J.G. Quintiere. Fire Saf. J. 26 (1996) 241-268.

[18]. J.L. Cordova, D.C. Walther, J.L. Torero, C. Fernandez-Pello. Combust. Sci. Technol. 164 (2001) 253-278.

[19]. C. Lautenberger, C.A. Fernandez-Pello. Approximate Analytical Solutions for the Transient Mass Loss Rate and Piloted Ignition Time of a Radiatively Heated Solid in the High Heat Flux Limit. In: Fire Safety Science – Proc. of the 8th Int. Symp., IAFSS, 2005, pp. 445-456.

[20]. B.T. Rhodes, J.G. Quintiere. Fire Saf. J. 26 (1996) 221-240.

[21]. J. Luche, T. Rogaume, F. Richard, E. Guillaume. Fire Saf. J. 46 (2011) 451-461.

[22]. R.S. Magee, R.D. Reitz. Proc. Combust. Inst. 15 (1975) 337-347.

[23]. A. Tewarson, S.D. Ogden. Combust. Flame 89 (1992) 237-259.